LAWRENCE
LIVERMORE
NATIONAL
LABORATORY

UCRL-JC-141757

Modeling of Short-Pulse-Driven Nickel-Like X-Ray Laser and Recent Experiments

J. Nilsen, J. Dunn

July 27, 2001

This article was submitted to *International Symposium on Optical Science and Technology, San Diego, CA, July 29 – August 3, 2001*

Modeling of short-pulse-driven nickel-like X-ray lasers and recent experiments

Joseph Nilsen and James Dunn

Lawrence Livermore National Laboratory, Livermore, CA 94550

ABSTRACT

The technique of using a nsec pulse to preform and ionize the plasma followed by a psec pulse to heat the plasma has enabled low-Z nickel-like ions to achieve saturated output when driven by small lasers with less than ten joules of energy. We model experiments done using the COMET laser at LLNL and the P102 laser at Limeil to produce Ni-like Pd and Ag lasers. The COMET experiments use a 2 J, 600 ps prepulse followed 700 psec later by a 6 J, 6 psec drive pulse in a 1.6 cm long line focus. The P102 experiments used a somewhat larger energy and were able to use different combinations of frequency doubled light for both the prepulse and short pulse drive. The LASNEX code is used to calculate the hydrodynamic evolution of the plasma and provide the temperatures and densities to the CRETIN code, which then does the kinetics calculations to determine the gain. The temporal and spatial evolution of the plasmas are studied both with and without radiation transport included to understand the role of the self photopumping process on the gain of the Ni-like 4f $\rightarrow$ 4d laser lines as well as the gain of the usual collisionally driven Ni-like 4d $\rightarrow$ 4p laser lines. In particular we study why the 4f $\rightarrow$ 4d line lases well only when frequency doubled light is used with the prepulse in the P102 experiments. Experimental results are presented for Ni-like Pd including two-dimensional near-field and far-field images.

Keywords: X-ray laser, prepulse technique

1. INTRODUCTION

Most researchers today use some variant of the prepulse technique [1-4] to achieve lasing in Ne-like or Ni-like ions. As a result the Ne-like 3p $^1S_0 \rightarrow 3s\ ^1P_1$ and Ni-like 4d $^1S_0 \rightarrow 4p\ ^1P_1$ laser lines now dominate the laser output. This technique illuminates solid targets with several pulses. The first pulse is used to create a large scale length plasma that is in the correct density range for gain and has sufficiently small density gradients for laser propagation. The subsequent pulses are then absorbed more efficiently and heat the plasma to lasing conditions. In this paper we model the Ni-like Ag experiments done with the P102 laser at Lemeil and the Ni-like Pd experiments done with the COMET laser at LLNL to understand the plasma conditions present and what gain is possible on different transitions. For the Ni-like Ag and Pd experiments we model the 4d $^1S_0 \rightarrow 4p\ ^1P_1$ line at 13.9 nm and 14.7 nm, respectively. In addition we model the photopumping mechanism [5] that drives the gain of the Ni-like Ag 4f $^1P_1 \rightarrow 4d\ ^1P_1$ line at 16.0 nm

2. PLASMA MODELING OF NI-LIKE AG EXPERIMENTS

To model the Ag experiments done at the P102 laser at Lemeil we did LASNEX one dimensional (1D) computer simulations of a Ag slab illuminated by a 5 J, 600 psec gaussian pulse followed 200 psec later by a 13 J, 0.5 psec gaussian pulse from a 1.05 μm Nd laser. The laser is focused to a 70 μm wide by 1.8-cm long line. The 200 psec delay between the

long and short pulse is peak to peak. The LASNEX calculations were 1D calculations but include an expansion angle of 15 degrees in the dimension perpendicular to the primary expansion so as to simulate 2D effects.

The LASNEX calculated densities and temperatures are used as input to the CRETIN code [6], which calculates the gains of the laser lines including radiation trapping effects for the four strong 4f and 4p → 3d resonance lines in Ni-like Ag. Bulk Doppler effects due to the expansion of the plasmas were also included. The Ag atomic model used by the CRETIN code includes all 107 detailed levels for levels up to n = 4 in Ni-like Ag.

Two dominant laser lines are predicted and these can be divided into two classes; the 4d $^1S_0 \rightarrow$ 4p $^1P_1$ line at 13.9 nm and the 4f $^1P_1 \rightarrow$ 4d $^1P_1$ line at 16.0 nm. The Ni-like 4d $^1S_0 \rightarrow$ 4p $^1P_1$ line lases by having monopole collisional excitation from the ground state populate the upper laser level. The lower laser level is depopulated by fast radiative decay to the ground state. Unlike the usual collisional excitation laser, the 4f $^1P_1 \rightarrow$ 4d $^1P_1$ line lases because radiation trapping allows a large radiation field to build up on the 3d $^1S_0 \rightarrow$ 4f $^1P_1$ resonance line and populate the 4f upper laser state by the self-photopumping process [5]. For convenience we leave out the $3d^9$ electrons which are common to both states.

In the experiments done at the P102 laser at Lemeil [7] one interesting result was that the 16.0 nm photopumped laser line was only observed when the long prepulse was frequency doubled. In this paper we present the modeling of the Ni-like Ag laser for the different cases where the long prepulse is frequency doubled (2ω) and when the fundamental frequency (1ω) is used. The long pulse energy is held constant. From these results we hope to gain some insight into the experimental observation.

Figure 1 shows the gain versus space and time for the 4d $^1S_0 \rightarrow$ 4p $^1P_1$ laser line at 13.9 nm for the nominal drive conditions described above for the two cases where the long prepulse is frequency doubled and when it is not. The short pulse optical drive laser peaks at 1 psec on this time scale so the evolution during the long pulse is not shown. The horizontal axis gives the distance from the target surface in the direction of the plasma expansion. The gray scale varies from 0 to 400 cm^{-1} with the darkest region representing gains greater than 400 cm^{-1}. With the frequency doubled (2ω) long pulse the gain region extends much further from the target surface and has a longer duration but there is certainly large gain available in both cases to produce lasing on this line.

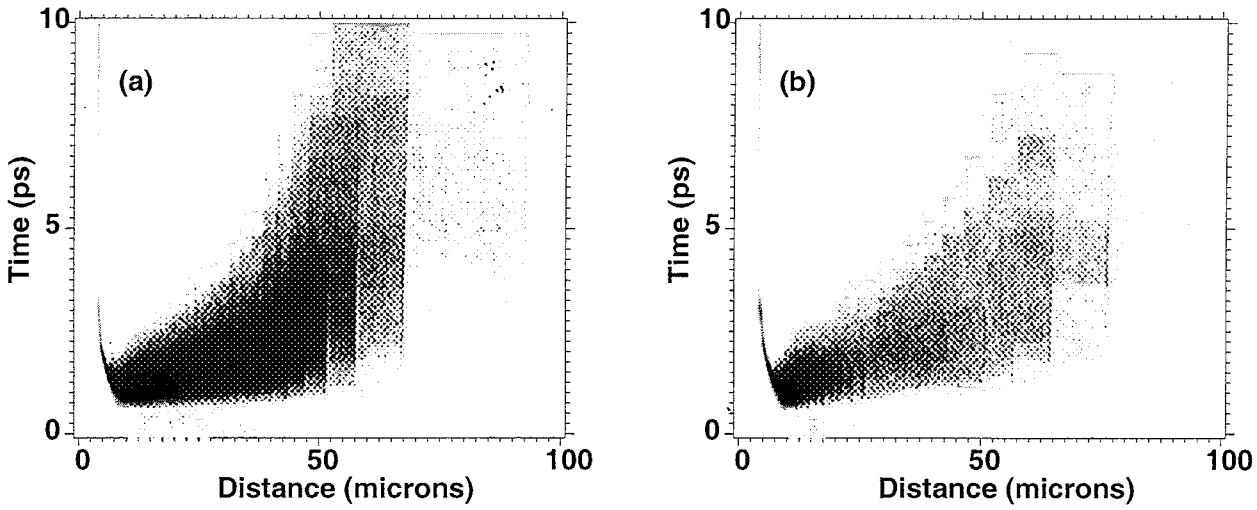

Fig. 1. Gain of the Ni-like Ag 4d $^1S_0$ - 4p $^1P_1$ laser line at 13.9 nm versus space and time for two cases; (a) uses 2ω long pulse while (b) uses 1ω long pulse. The gray scale varies from 0 to 400 with the darkest region representing gain greater than 400 cm^{-1}. The short pulse optical laser peaks at 1 ps on the time axis.

If we look at typical conditions in the plasma for the 2ω case, at 2 psec in Fig. 1 (a) the gain of the 13.9 nm line peaks at a distance of 39 μm with a value of 285 cm^{-1}. At this position the electron temperature is 928 eV with an ion temperature of 98 eV. The electron density is 1.9 x 10^{20} cm^{-3} and the gradient in the electron density is –8.9 x 10^{22} cm^{-4}. For a 1-cm length the X-ray laser would refract an additional 39 μm from target surface so clearly the gradients are important in these high gain regions. However with such high gains one could reach saturation with much shorter targets. The lower gain regions with lower gradients also contribute strongly to the laser output. Clearly more work needs to be done to simulate these cases including doing laser propagation calculations to estimate the laser intensity under different conditions.

If we now look at the gain for the 4f $^1P_1 \rightarrow$ 4d $^1P_1$ line at 16.0 nm, Fig. 2 shows the gain for this line under the two cases where the long prepulse is frequency doubled and when it is not. Since the gain is more confined in space and time for this line we plot a smaller region in space and time. For the frequency doubled case (a) the gain is quite large over a large spatial region and it is not surprising that this line can be strong and even dominate the output as has been observed in recent experiments [7]. The time duration is shorter for this line as compared with the 13.9 nm line so the traveling wave geometry is even more important in making this line lase. Using the fundamental frequency for the long pulse, Fig. 2 (b), results in a high gain over a very narrow region in space and time so it is not surprising that no significant lasing is seen

If one looks at the temperature evolution of the preplasma for the two different prepulse cases one calculates that the electron temperature is hotter for the 1ω long pulse compared to the 2ω case. This has several implications. First, the hotter preplasma tends to be overionized in the density region that is most likely to lase. The hotter preplasma also has less absorption for the short pulse. For the 2ω case the colder plasma absorbs the short pulse better and results in a hotter plasma for driving the gain. The hotter plasma also builds up a stronger pump strength on the 4f $^1P_1 \rightarrow$ 3d $^1S_0$ resonance line that drives the gain on the 16.0 nm laser line.

To understand the role of the self-photopumping process on the gain of the 4f $^1P_1 \rightarrow$ 4d $^1P_1$ line we also did calculations without the inclusion of line transport on the 4f – 3d lines. Figure 3 shows a comparison of the gain with and without the line transport included. By turning off the line transport calculation the 4f and 4p → 3d resonance lines become optically thin and have no line strength. In this case the gain of the 4f $^1P_1 \rightarrow$ 4d $^1P_1$ line essentially disappears except in a very narrow region near the critical density surface. This gain region is very small and short-lived and has steep gradients that would make it difficult to propagate any significant distance.

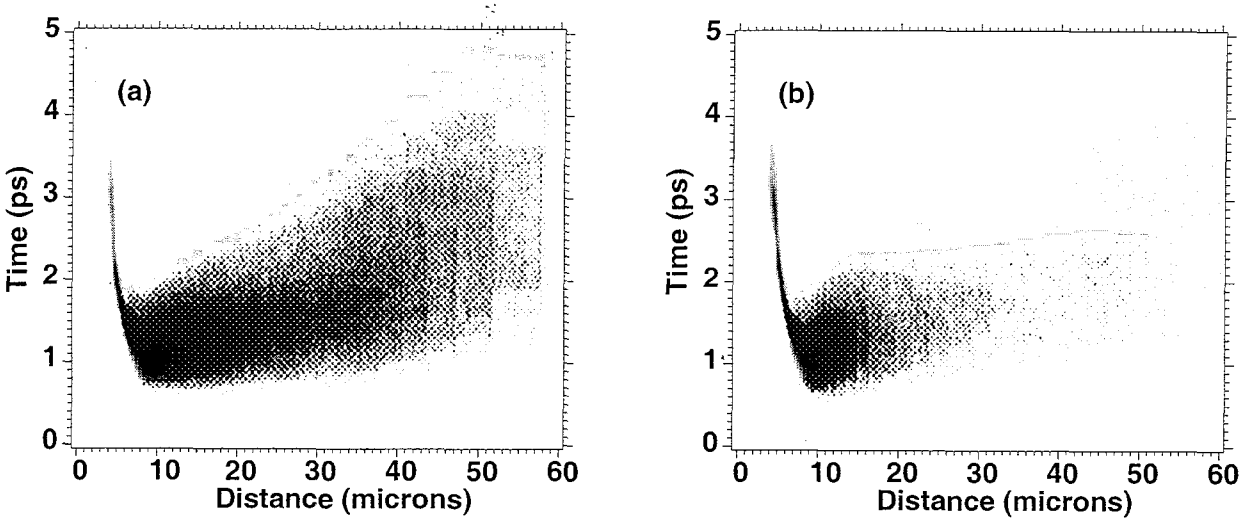

Fig. 2. Gain of the Ni-like Ag 4f $^1P_1$ - 4d $^1P_1$ laser line at 16.0 nm versus space and time for two cases; (a) uses 2ω long pulse while (b) uses 1ω long pulse. The gray scale varies from 0 to 400 with the darkest region representing gain greater than 400 cm^{-1}. The short pulse optical laser peaks at 1 ps on the time axis.

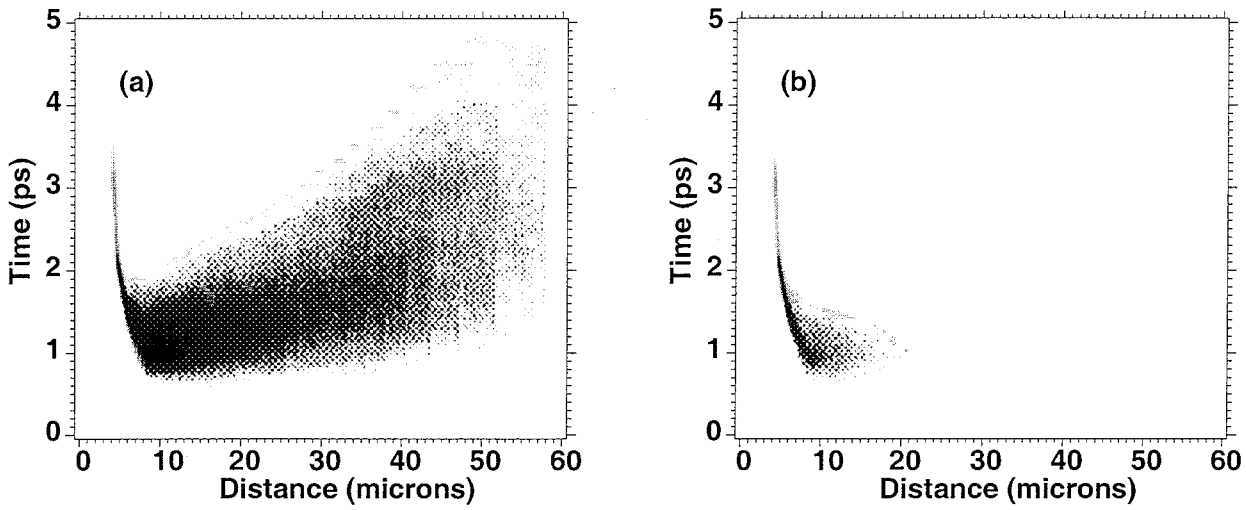

Fig. 3. Gain of the Ni-like Ag 4f $^1P_1$ - 4d $^1P_1$ laser line at 16.0 nm versus space and time for two cases; line transport is tunred on (a) and off (b). Without the photopumping process the gain disappears except in a very narrow region near the critical density surface. The gray scale varies from 0 to 400 with the darkest region representing gain greater than 400 cm^{-1}. The short pulse optical laser peaks at 1 ps on the time axis.

Calculations were also done using 3ω and 4ω long pulses while holding the long pulse energy constant. Those calculations suggest that the gain may improve even more using the 3ω long pulse. We also tried reducing the energy of the long pulse for the 1ω case so as to achieve a better ionization balance. While this did improve the predicted gain it still was not as good as the 2ω case, one reason being that the preplasma was smaller. One challenge with optimizing the long prepulse conditions is to create a preplasma while not overionizing the plasma. Use of the higher frequency long pulse gives one more flexibility in achieving the optimum conditions for lasing.

3. NI-LIKE PD EXPERIMENTS AND MODELING

The Pd laser experiments were performed on the Compact Multipulse Terawatt (COMET) laser system at LLNL [8]. This laser, operating at 1054 nm wavelength, utilizes the technique of CPA to produce two beams of nominally 500 fs and 600 ps (FWHM) pulse duration with a repetition rate of 1 shot every 4 minutes. The short pulse was lengthened to 6 ps with an energy of 6 to 7 J while the long pulse energy was typically 1 to 2 J delivered in the line focus at the target chamber. The laser spectrum, energy in the two laser pulses, the short pulse near-field beam profile, the pulse shapes and relative delay were monitored on every shot. The peak-to-peak delay between the laser pulses was found to be optimal at 700 ps with the short pulse arriving after the long pulse. The line focus length of 1.6 cm was achieved with a cylindrical lens and an on-axis paraboloid. The short pulse beam was focused to 120 μm while the long pulse was defocused by a factor of two. The long pulse was defocused to produce a more uniform lateral plasma medium and increase absorption prior to the excitation process driven by the picosecond laser. More importantly, a traveling wave scheme was introduced to mitigate against the reduced amplification at longer target lengths resulting from the short-lived transient gain lifetime and increase the laser output. The traveling wave optic consisted of seven flat mirror segments placed before the focusing optics.

In previous experiments we have demonstrated saturated output on the Ni-like Pd 4d $^1S_0 \rightarrow$ 4p $^1P_1$ laser line at 14.7 nm as well as other Ni-like ions from Nb to Ag [8,9]. In this paper we present the first near-field and far-field images of the Ni-

like Pd laser line at 14.7 nm. For the far-field measurements two flat Mo:Si multilayer mirrors optics (a 0° and a 45° flat mirror) are used to direct the X-ray laser into the CCD camera. The 0° mirror is pointed 0.54° away from the Pd target surface in order to send the X-ray laser clear of the plasma plume. Therefore the X-ray laser strikes the 45° mirror at an angle of 45.54°. The CCD camera is 130.4 cm from the end of the target. A filter of 1900 Å thick Zr coated on 1000Å thick polyimide substrate is placed between the X-ray laser target and the first multilayer mirror. The X-ray laser is double passed through this first filter. A second filter of 3000 Å thick Zr coated on 1000 Å thick polyimide substrate is placed before the CCD camera. The filters block the optical light as well as protect the multilayer mirrors from damage. The CCD camera is intrinsically 1024 by 1024 pixels with a 24-μm pixel size. For the far-field measurement we average every 2 pixels and only record 512 by 512 pixels from the CCD camera. This makes each pixel 48 μm in size, which corresponds to 36.8 μrad per pixel in the data. Fig. 4 (a) shows the far field pattern for the Ni-like Pd laser using 1.88 J in the long pulse and 6.67 J in the short pulse. The horizontal divergence is about 3 mrad in the plasma expansion direction while the vertical divergence is larger, about 6 mrad in the line focus direction.

We also obtained near field X-ray laser images by using a spherical Mo:Si multilayer mirror with a focal length of 11.75cm that was placed 12.33 cm from the end of the Pd X-ray laser target. A flat multilayer mirror oriented at 45° was used to send the X-ray laser beam into the CCD camera. The CCD camera was 248.1 cm from the spherical curved mirror resulting in a magnification of 20. A 2000Å thick Lexan filter coated with 750Å of Al was placed between the X-ray laser target and the spherical Mo:Si multilayer mirror. The X-ray laser is double passed through this first filter. This results in substantial attenuation in the X-ray laser, as expected. A second filter of 2952 Å thick Zr coated on 1050Å thick polyimide was placed before the CCD camera to block the optical light. Fig. 4 (b) shows the near-field pattern for the Ni-like Pd laser line at 14.7 nm using 1.27 J in the long pulse and 6.58 J in the short pulse. The horizontal direction is the plasma expansion

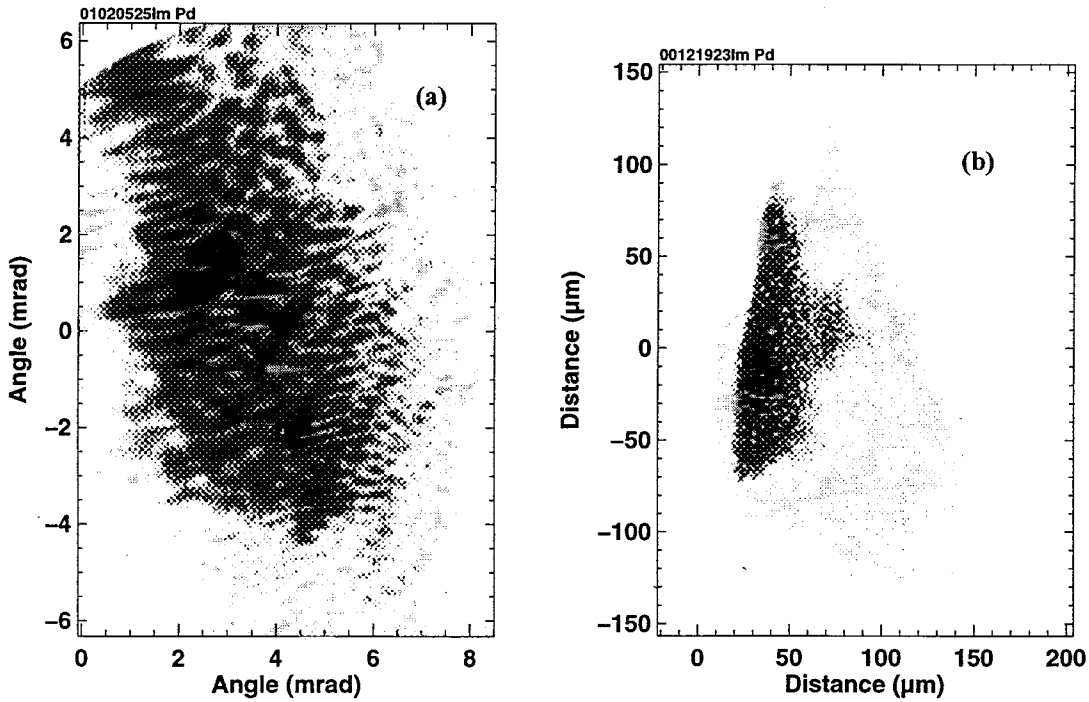

Fig. 4. Far-field image (a) and near-field image (b) of the Ni-like Pd 4d $^1S_0$ - 4p $^1P_1$ laser output at 14.7 nm. In both images the plasma expansion direction is in the horizontal direction while the line focus is in the vertical direction. In the near-field image the plasma is expanding to the right with the target surface estimated to be near 0 μm based on plasma emission.

direction. The laser emission is quite narrow in this direction. Looking at the plasma emission, the target surface is estimated to be at 0 μm on this scale. However a better fiducial is needed to determine the absolute target surface. The vertical direction is the line focus direction and the laser emission region is determined by the width of the line focus and is about five times larger than the expansion direction.

To model the Pd experiments done at COMET we did LASNEX one dimensional (1D) computer simulations of a Pd slab illuminated by a 2 J, 600 psec gaussian pulse followed 700 psec later by a 6 J, 6 psec gaussian pulse from a 1.05 μm Nd laser. The laser is focused to a 120 μm wide by 1.6 cm long line. The 700 psec delay between the long and short pulse is peak to peak. The LASNEX calculations were 1D calculations but include an expansion angle of 15 degrees in the dimension perpendicular to the primary expansion so as to simulate 2D effects. Since the long pulse is defocused by a factor of 2 in the experiments we reduced the long pulse energy in the calculation to 1J.

The LASNEX calculated densities and temperatures are used as input to the CRETIN code [6], which calculates the gains of the laser lines including radiation trapping effects for the four strong 4f and 4p → 3d resonance lines in Ni-like Pd. Bulk Doppler effects due to the expansion of the plasmas were also included. The Pd atomic model used by the CRETIN code includes all 107 detailed levels for levels up to n = 4 in Ni-like Pd.

Two dominant laser lines are predicted and these can be divided into two classes. The 4d $^1S_0 \rightarrow$ 4p $^1P_1$ line at 14.7 nm and the 4f $^1P_1 \rightarrow$ 4d $^1P_1$ line at 17.0 nm. The Ni-like 4d $^1S_0 \rightarrow$ 4p $^1P_1$ line lases by having monopole collisional excitation from the ground state populate the upper laser level. The lower laser level is depopulated by fast radiative decay to the ground state. Unlike the usual collisional excitation laser, the 4f $^1P_1 \rightarrow$ 4d $^1P_1$ line lases because radiation trapping allows a large radiation field to build up on the 3d $^1S_0 \rightarrow$ 4f $^1P_1$ resonance line and populate the 4f upper laser state by the self-photopumping process. Figure 5 shows the gain versus space and time for the 4d $^1S_0 \rightarrow$ 4p $^1P_1$ laser line at 14.7 nm and the 4f $^1P_1 \rightarrow$ 4d $^1P_1$ line at 17.0 nm. The short pulse optical drive laser peaks at 6 psec on this time scale so the evolution during the long pulse is not shown. The gray scale varies from 0 to 400 cm^{-1} with the darkest region representing gains greater than 400 cm^{-1}. The 17 nm line is much weaker and is observed only weakly in the COMET experiments for Pd. It has been observed more strongly for lower Z materials such as Mo [9] under the COMET conditions. The 14.7 nm line is predicted to be quite strong. The calculations predict a very strong gain region 20 to 30 μm from the target surface that is similar to what is observed in the experiments. Laser propagation calculations still need to be done to predict the influence of refraction and amplification on the laser output.

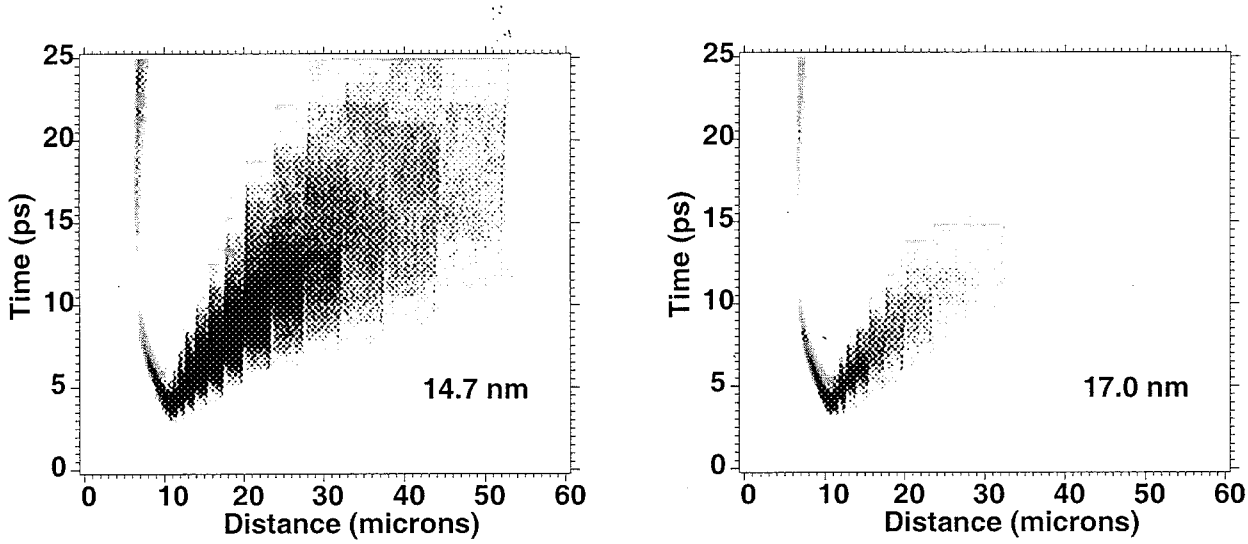

Fig. 5. Gain of the Ni-like Pd 4d $^1S_0$ - 4p $^1P_1$ laser line at 14.7 nm and the 4f $^1P_1$ - 4d $^1P_1$ laser line at 17.0 nm versus space and time. The gray scale varies from 0 to 400 with the darkest region representing gain greater than 400 cm^{-1}. The short pulse optical laser peaks at 6 ps on the time axis.

4. CONCLUSIONS

In this work we model experiments done using the COMET laser at LLNL and the P102 laser at Limeil to produce Ni-like Pd and Ag lasers. The COMET experiments use a 2 J, 600 ps prepulse followed 700 psec later by a 6 J, 6 psec drive pulse in a 1.6 cm long line focus. The P102 experiments used a 5 J, 600 psec gaussian pulse followed 200 psec later by a 13 J, 0.5 psec gaussian pulse from a 1.05 μm Nd laser. The P102 experiments were able to use different combinations of frequency doubled light for both the prepulse and short pulse drive. The LASNEX code was used to calculate the hydrodynamic evolution of the plasma and provide the temperatures and densities to the CRETIN code, which then did the kinetics calculations to determine the gain. The temporal and spatial evolution of the plasmas were studied both with and without radiation transport included to show the essential role of the self-photopumping process on the gain of the Ni-like 4f $\rightarrow$ 4d laser lines as well as the gain of the collisionally driven Ni-like 4d $\rightarrow$ 4p laser lines. In particular we discussed why the Ni-like Ag 4f $\rightarrow$4d line lases well only when frequency doubled light is used with the prepulse in the P102 experiments. Two-dimensional near-field and far-field images were presented for Ni-like Pd and the near-field images were compared with calculations.

ACKNOWLEDGEMENTS

The authors would like to thank Richard A. Ward, Charles P. Verdon, and Albert L. Osterheld for their support. We also wish to thank Howard A. Scott for his assistance in learning the CRETIN code and implementing requested changes in the code. Work performed under the auspices of the U. S. Department of Energy by the University of California Lawrence Livermore National Laboratory under contract No.W-7405-ENG-48.

REFERENCES

[1] J. Nilsen, B. J. MacGowan, L. B. Da Silva, and J. C. Moreno, "Prepulse technique for producing low-Z Ne-like X-ray lasers," *Phys. Rev. A* **48**, 4682 - 4685 (1993).

[2] J. C. Moreno, J. Nilsen, and L. B. da Silva, "Traveling wave excitation and amplification of neon-like germanium 3p - 3s transitions," *Opt. Comm.* **110**, 585 - 589 (1994).

[3] P. V. Nickles, V. N. Shlyaptsev, M. Kalachnikov, M. Schnuerer, I. Will, and W. Sandner, "Short pulse X-ray laser at 32.6 nm based on transient gain in Ne-like titanium," *Phys. Rev. Lett.* **78**, 2748 – 2751 (1997).

[4] J. Nilsen, Y. L. Li, and J. Dunn, "Modeling psec-laser-driven neon-like titanium X-ray laser experiments," *J. Opt. Soc. Am. B* **17**, 1084-1092 (2000).

[5] J. Nilsen, J. Dunn, A. L. Osterheld, and Y. L. Li, "Lasing on the self photopumped nickel-like 4f $^1P_1 \rightarrow$ 4d $^1P_1$ X-ray transition," *Phys. Rev. A* **60**, R2677 – 2680 (October 1999).

[6] H.A. Scott, "Cretin - a radiative transfer capability for laboratory plasmas," *JQSRT* **71**, 689-701 (2001).

[7] J. Kuba, A. Klisnick, D. Ros, P. Fourcade, G. Jamelot, J. L. Miquel, N. Blanchot, J. F. Wyart, "Two-color transient pumping in Ni-like silver at 13.9 and 16.1 nm," *Phys. Rev. A.* **62**, 043808 (2000)

[8] J. Dunn, Y. Li, A. L. Osterheld, J. Nilsen, J. R. Hunter, and V. N. Shlyaptsev, "Gain saturation regime for laser-driven tabletop, transient Ni-like ion x-ray lasers," *Phys. Rev. Lett.* **84**, 4834 – 4837 (2000).

[9] Y. L. Li, J. Dunn, J. Nilsen, T. W. Barbee, Jr., A. L. Osterheld, and V. N. Shlyaptsev, "A saturated table-top X-ray laser system at 19 nm," *J. Opt. Soc. Am. B* **17**, 1098-1101 (2000).